# Acrofacial Dysostosis, Cincinnati Type, a Mandibulofacial Dysostosis Syndrome with Limb Anomalies, Is Caused by *POLR1A* Dysfunction

K. Nicole Weaver,[1,9,*] Kristin E. Noack Watt,[2,3,9] Robert B. Hufnagel,[1] Joaquin Navajas Acedo,[2] Luke L. Linscott,[4] Kristen L. Sund,[1] Patricia L. Bender,[1] Rainer König,[5] Charles M. Lourenco,[6] Ute Hehr,[7] Robert J. Hopkin,[1] Dietmar R. Lohmann,[8] Paul A. Trainor,[2,3,10] Dagmar Wieczorek,[8,10] and Howard M. Saal[1,10]

We report three individuals with a cranioskeletal malformation syndrome that we define as acrofacial dysostosis, Cincinnati type. Each individual has a heterozygous mutation in *POLR1A*, which encodes a core component of RNA polymerase 1. All three individuals exhibit varying degrees of mandibulofacial dysostosis, and two additionally have limb anomalies. Consistent with this observation, we discovered that *polr1a* mutant zebrafish exhibited cranioskeletal anomalies mimicking the human phenotype. *polr1a* loss of function led to perturbed ribosome biogenesis and p53-dependent cell death, resulting in a deficiency of neural-crest-derived skeletal precursor cells and consequently craniofacial anomalies. Our findings expand the genotypic and phenotypic heterogeneity of congenital acrofacial disorders caused by disruption of ribosome biogenesis.

## Introduction

The skeleton provides a structural framework in vertebrates for muscle attachments, facilitating movement, protecting vital organs, and maintaining homeostasis of the immune and vascular systems. Perturbation of bone development results in congenital craniofacial and skeletal anomalies, which affect approximately 1 in 3,000 live births.[1] One specific type of congenital skeletal disorder, termed facial dysostosis, describes a set of clinically and etiologically heterogeneous anomalies of the craniofacial skeleton, and they arise as a consequence of abnormal development of the first and second pharyngeal arches and their derivatives during embryogenesis. Mandibulofacial dysostosis and acrofacial dysostosis are subgroups of human facial dysostoses.[2] The best-understood mandibulofacial dysostosis, Treacher Collins syndrome (MIM: 154500), is a genetically heterogeneous disorder caused by mutations in at least three genes—*TCOF1* (MIM: 606847), *POLR1C* (MIM: 610060), and *POLR1D* (MIM: 613715)—which regulate rDNA transcription and ribosome biogenesis.[3–5] The acrofacial dysostoses, which include at least six genetically and phenotypically distinct subtypes,[2] encompass similar craniofacial anomalies with the addition of limb defects.[6] Moreover, perturbed ribosome biogenesis has also been associated with the pathogenesis of acrofacial dysostosis, Nager type (MIM: 154400).[7,8]

Here, we present three individuals with mandibulofacial dysostosis; two have limb anomalies, and all have putative pathogenic variants in *POLR1A* (GenBank: NM_015425.3). We describe the spatiotemporal expression of *polr1a* in zebrafish and characterize the phenotype of zebrafish with *polr1a* loss of function. Further studies demonstrated that altered *POLR1A* function has deleterious effects on ribosome biogenesis. Our findings document acrofacial dysostosis, Cincinnati type as a syndrome characterized by a spectrum of mandibulofacial dysostosis phenotypes (with or without extrafacial skeletal defects) caused by abnormal function of *POLR1A*.

## Material and Methods

### Whole-Exome Sequencing

DNA specimens were collected according to protocols approved by the institutional review board at Cincinnati Children's Hospital Medical Center. Informed consent for DNA storage and genetic analyses was obtained from all subjects. Whole-genome DNA was extracted from whole blood by standard methods. Library construction was performed on double-stranded DNA (sheared by sonication to an average size of 200 bp) in an automated fashion on an IntegenX Apollo324. After nine cycles of PCR amplification by the Clontech Advantage II Kit, 1 μg of genomic library was recovered for exome enrichment with the NimbleGen EZ Exome V2 Kit. Libraries were sequenced on an

[1]Division of Human Genetics, Department of Pediatrics, Cincinnati Children's Hospital Medical Center and University of Cincinnati College of Medicine, MLC 4006, 3333 Burnet Avenue, Cincinnati, OH 45229, USA; [2]Stowers Institute for Medical Research, 1000 East 50th Street, Kansas City, MI 64110, USA; [3]University of Kansas Medical Center, Kansas City, MI 66160, USA; [4]Department of Radiology, Cincinnati Children's Hospital Medical Center, Cincinnati, OH 45229, USA; [5]Institut für Humangenetik, Universitätsklinikum Frankfurt, Theodor-Stern-Kai 7, 60596 Frankfurt, Germany; [6]Neurogenetics Unit, Clinics Hospital of Ribeirao Preto, University of Sao Paulo, Avenue Bandeirantes 3900, Sao Paulo 14049-900, Brazil; [7]Zentrum für Humangenetik, Universitätsklinikum Regensburg, Franz-Josef-StrauB-Allee 11, 93053 Regensburg, Germany; [8]Institut für Humangenetik, Universitätsklinikum Essen, Universität Duisburg-Essen, Hufelandstr 55, 45122 Essen, Germany
[9]These authors contributed equally to this work
[10]These authors contributed equally to this work
*Correspondence: kathryn.weaver@cchmc.org
http://dx.doi.org/10.1016/j.ajhg.2015.03.011. 

Illumina HiSeq 2500, generating approximately 30 million paired-end reads, each 100 bases long. Data analysis utilized the Broad Institute's Genome Analysis Toolkit (GATK).[9] Reads were aligned with the Illumina Chastity Filter with the Burrows-Wheeler Aligner (BWA).[10] Variant sites were called with the GATK UnifiedGenotyper module. Single-nucleotide-variant calls were filtered by variant quality-score recalibration.[9] Filtering of variants was performed with Golden Helix's SNP & Variation Suite.

### Sanger Sequencing

Sanger sequencing was performed by standard methods on exons 1–34 of *POLR1A*. Primers were designed with Primer3 and are listed in Tables S1 and S2. PCR products were amplified with 50 ng of DNA and standard PCR reagents on an ABI Veriti Thermocycler (Applied Biosystems). PCR products were precipitated, and sequencing PCR was performed with BigDye Terminator Ready Reaction Mix (ABI Biosystems).

Clustal Omega was used for analysis of homology between human and *Saccharomyces cerevisiae* A190 proteins.[11–13]

### Zebrafish Embryos

Zebrafish (*Danio rerio*) embryos were raised at 28.5°C and staged as described in Kimmel et al.[14] The AB strain was used as the wild-type strain. Heterozygous *polr1a*$^{hi3639Tg}$ fish[15,16] were identified with primers 5′-CTCCCAGAACACAGTCACACG-3′ and 5′-GCTAGCTTGCCAAACCTACAGGT-3′ and incrossed for the generation of homozygous mutant embryos. Homozygous mutant embryos were identified by morphology and then confirmed by PCR. Transgenic Tg(7.2 kb-*sox10:gfp*) zebrafish,[17] referred to as *sox10:gfp*, were crossed to *polr1a* heterozygotes for visualization of neural crest cells (NCCs) in *polr1a* mutant embryos and controls.

### Phenotypic Analyses

In situ hybridization was performed according to standard protocols. A portion of *polr1a* was amplified with primers 5′-CTCCGCTGATGAAACAAGAAA-3′ (forward) and 5′-CAAACGATTAATAGGCCTGTACCTG-3′ (reverse) and cloned into the TOPO II vector (Invitrogen), which was used for generating the *polr1a* probe. Embryos were mounted and imaged with a Leica MZ16 microscope equipped with a Nikon DS-Ri1 camera and NIS Elements BR 3.2 imaging software.

Alcian blue and Alizarin red staining were performed as described in Walker and Kimmel[18] and imaged with the same system described previously.

Immunostaining for HuC (1:200; Invitrogen) and Sox10 (1:500; Genetex) with Alexa 488 secondary antibody (1:500; Invitrogen) was performed as described in Westerfield.[19] TUNEL was completed as described in Crump et al.[20] with slight modifications. Embryos were permeabilized overnight in methanol at −20°C and incubated for 1 hr at 37°C in a reaction mixture containing TdT and TMR red. Embryos were imaged with a Zeiss upright 700 confocal microscope, and images were taken and processed with Zen software.

### Molecular Analyses

RNA was collected from zebrafish at 24 hr post-fertilization (hpf) with the QIAGEN miRNeasy Micro Kit and was tested for quality on an Agilent 2100 Bioanalyzer. The Superscript III Kit (Invitrogen) was used to synthesize cDNA for qRT-PCR. Primers for *polr1a* were 5′-CACCTGGAGAAGAAATCCAAG-3′ and 5′-GATGTGCTTGACAGGGTCAG-3′, and primers for *tp53* were 5′-CGAGCCACTGCCATCTATAAG-3′ and 5′-TGCCCTCCACTCTTATCAAATG-3′. rRNA primer sequences were obtained from Azuma et al.[21] Power Sybr (Life Technologies) reaction mix and the ABI 7900HT real-time PCR cycler were used for measuring cDNA amplification. Data were analyzed with Biogazelle software, and the Mann-Whitney test was used for determining statistical significance.

Protein samples of 100 fish/sample were collected at 24 hpf and 4 days post-fertilization (dpf). 24-hpf zebrafish were deyolked prior to protein extraction. Embryos were homogenized and suspended in sample buffer according to standard protocols.[19] Primary antibodies used were zebrafish Tp53 (1:500, Anaspec) and α-tubulin (1:10,000, Sigma). Fluorescent secondary antibodies (Alexa 680 anti-mouse and Alexa 800 anti-rabbit, Invitrogen) were used at a dilution of 1:20,000. Images were taken with the LICOR system and then quantified with ImageJ. Tp53 amounts were normalized to those of α-tubulin, and statistical significance was determined with Student's t test.

## Results

### Human Phenotypes

Individual 1A1 is a 3-year-old white male with multiple prenatally identified craniofacial anomalies, including severe micrognathia, which required tracheostomy at birth to establish a secure airway. Initial physical exam of the full-term newborn revealed down-slanting palpebral fissures, severe bilateral lower eyelid clefts, inferiorly displaced orbits, an underdeveloped midface, and extreme micrognathia (Figures 1A–1C). Bilateral anotia and severe conductive hearing loss were present. At birth, head circumference was 33 cm (−1.7 SDs), length was 43 cm (−4 SDs), and weight was 2.4 kg (−2.5 SDs). Short stature became more significant with age (height was 76 cm [−5 SDs] at age 3 years). Hypoplasia of the zygomatic arches, maxilla, and mandible with absent mandibular rami was seen on a computed-tomography (CT) scan (Figures 1D and 1E). In addition, individual 1A1 had congenital short bowed femurs with metaphyseal flaring, dysplastic acetabulae, and delayed or absent ossification of the capital femoral epiphyses (Figure 1F). His parents are healthy, and he has no siblings. Individual 1A2, previously described by Wieczorek et al.,[22] is a 6-year-old Brazilian female with craniofacial anomalies including short, down-slanting palpebral fissures, upper and lower eyelid clefts, absent medial eyelashes, heminasal aplasia, large ears, and full lips (Figure 2A). Her facial CT scan demonstrated hypoplastic zygomata and maxilla and bilateral choanal atresia, which was more severe on the left side (Figures 2B and 2C). Growth parameters were significant for microcephaly (45.5 cm [−4.3 SDs]), and height (110.4 cm [−1.4 SDs]) and weight (15.4 kg) were normal. Individual 1A3 is a 52-year-old German male with facial dysmorphism including down-slanting palpebral fissures, malar flattening, micrognathia, and low-set ears with a unilateral dysplastic helix and accessory tragus (Figures 2D and 2E). On examination, he had short, broad fingers (Figure 2F) and toes, and his height, weight, and head circumference were within normal limits. His parents,

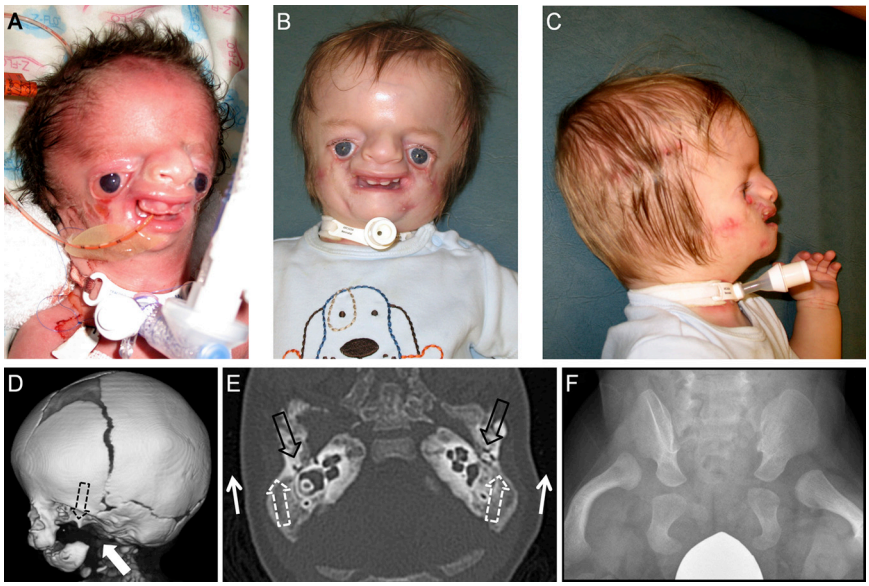


**Figure 1. Individual 1A1**
(A) Newborn photo demonstrates extensive craniofacial malformations.
(B and C) Frontal and profile images were taken at age 18 months after multiple reconstructive surgeries.
(D) 3D reformatted image demonstrates severe maxillary and zygomatic hypoplasia (black open dashed arrow) and severe micrognathia and retrognathia (white block arrow).
(E) Axial CT of the temporal bones demonstrates severe microtia with absent pinnae (white arrows), external auditory atresia (white open dashed arrows), and severe middle-ear hypoplasia and ossicular dysplasia (black open arrows).
(F) X-ray of individual 1A1 demonstrates bilateral hip dysplasia and anterior bowing deformity of the femurs.

four siblings, and two sons are healthy. His parents are reported to be consanguineous, but the degree is unknown. Clinical features of all three affected individuals are summarized in Table 1.

### Sequencing Results

Clinical *TCOF1* sequencing and SNP microarray (Illumina HD HumanOmni1-Q uad BeadChip Kit) of individual 1A1 did not identify abnormalities. Individual 1A2 had a normal karyotype and Affymetrix Cytoscan HD Array. Additionally, sequencing of *TCOF1*, *POLR1D*, *POLR1C*, and *TXNL4* did not detect pathogenic variants, nor did multiplex ligation-dependent probe amplification of *TXNL4* and *TCOF1*. Sequencing of *TCOF1* in individual 1A3 did not detect a mutation.

Whole-exome sequencing of individual 1A1 revealed a de novo heterozygous *POLR1A* variant (c.1777G>C [p.Glu593Gln]; GenBank: NM_015425.3), which was validated by Sanger sequencing (Figure S1A). The variant was not present in control data from 1000 Genomes,[23] the NHLBI ESP6500 dataset,[24] and approximately 300 in-house control exomes. The affected amino acid is highly conserved among seven species (Table S3), and the variant is predicted to be pathogenic by in silico models (Table S4). Two additional de novo variants were identified in *FN1* (MIM: 135600) and *KANSL3*. Neither variant is predicted to be pathogenic. *KANSL3* mutations are not associated with a known phenotype. Mutations in *FN1* cause autosomal-dominant glomerulopathy with fibronectin deposits (MIM: 601894), which was not present in individual 1A1. For excluding the possibility of a second genetic diagnosis, the exome data were filtered for homozygous recessive and compound-heterozygous variants. No additional candidate variants were identified (see Table S5 for a breakdown of the filtering strategy and results).

After identification of *POLR1A* as a candidate gene, targeted Sanger sequencing of *POLR1A* was performed in 48 individuals with mandibulofacial dysostosis of unknown genetic etiology. Individual 1A2 had a heterozygous *POLR1A* frameshift variant (c.3649delC [p.Gln1217Argfs*10]; Figure S1B), which was inherited from her father, who has down-slanting palpebral fissures and mild malar hypoplasia. Individual IA-3 had a heterozygous missense variant (c.3895G>T [p.Val1299Phe]) in *POLR1A* (Figure S1C). His parents were not available for testing. The *POLR1A* variants identified in individuals 1A2 and 1A3 are predicted to be pathogenic by in silico models, and neither has been reported in control populations from dbSNP or NHLBI ESP6500 (see Tables S4 and S6 for in silico predictions and conservation).

### *Polr1a* Expression and Functional Studies

In order to understand how dysfunction of *POLR1A* causes skeletal malformations, we investigated the expression and function of *polr1a* by using zebrafish as a model. In situ hybridization revealed that *polr1a* was dynamically expressed during zebrafish embryogenesis (Figure 3). *polr1a* expression was initiated as early as the 2-cell stage and continued to be ubiquitously expressed until at least 12 hpf. By 18 hpf, the expression of *polr1a* became enriched in the eyes and brain. The tissue specificity of *polr1a* expression continued at 24 hpf in regions of the brain, eyes, otic vesicles, and somites. Beyond 36 hpf, *polr1a* expression was diminished throughout the embryo but was maintained at the midbrain-hindbrain boundary and the ocular lens.

To explore the function of *polr1a* during craniofacial and limb development, we examined zebrafish with an insertion mutation[15,16] in the 5′ UTR of *polr1a* (*polr1a*$^{hi3639Tg}$). This mutation results in a severe loss of *polr1a* expression in homozygous mutant embryos (Figure S2). Early in development, however, these embryos are not completely without Polr1a because of the maternal contribution of *polr1a*. Homozygous *polr1a* mutant embryos exhibited gross morphological defects from 15 hpf onward (Figure 4).

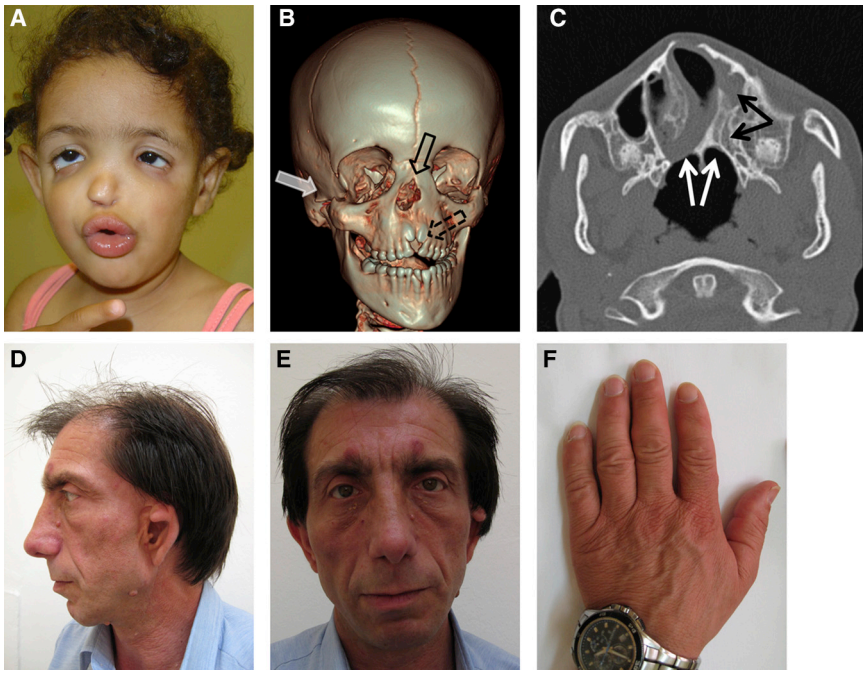


**Figure 2. Individuals 1A2 and 1A3**
(A) Individual IA2 at 6 years of age.
(B) 3D bone image of individual IA2 demonstrates moderate zygomatic hypoplasia (white block arrow), midface hypoplasia with absent nasal bones (white open arrow), and midline alveolar process hypoplasia (open white dashed arrow).
(C) Axial CT image of individual IA2 demonstrates bilateral choanal atresia (white arrows) and left maxillary and ethmoid sinus hypoplasia (black arrows).
(D and E) Individual 1A3 at 52 years of age. Profile and frontal photos demonstrate subtle craniofacial dysmorphism including malar hypoplasia, micrognathia, and dysplastic ears.
(F) Short, broad fingers of individual IA3.

Compared to wild-type controls, the *polr1a* mutants had noticeably smaller and misshapen heads. By 24 hpf, the craniofacial phenotype in *polr1a* mutant embryos became more pronounced. Not only was the head considerably smaller, but the eyes and brain were also abnormally shaped. In addition, the tail was short and misshapen. A pattern of dark, grainy cells could be observed in the head and at the end of the tail, suggestive of cell death as a component underlying the pathogenesis of the phenotype. The phenotype continued to progress such that by 36–48 hpf, *polr1a* mutant embryos were proportionally smaller than wild-type controls and exhibited microphthalmia, cerebral hypoplasia, jaw agenesis, perturbed pigmentation, and abnormal morphology of the heart, otolith, and pectoral fin. *polr1a* mutant fish died by 4–5 dpf, and skeletal staining revealed that *polr1a* mutant zebrafish had reduced NCC-derived cartilage at 5 dpf (Figure 5), consistent with jaw agenesis.

The vertebrate craniofacial skeleton is derived primarily from NCCs, a migratory progenitor cell population.[25] Given the craniofacial phenotypes observed in *polr1a* mutant zebrafish and in the three humans with acrofacial dysostosis, Cincinnati type, we hypothesized that *polr1a* is functionally required in NCC development. We examined *polr1a* mutant embryos for evidence of defects in NCC formation, migration, and differentiation (Figure 6). By 12 hpf, the neural plate appeared normal in *polr1a* mutant embryos, as evidenced by the normal pattern of *sox2* expression. However, altered expression of *sox10*, which demarcates NCCs migrating from the neural plate, was coincident with the craniofacial phenotype. The number of *sox10*-positive migratory NCCs was noticeably lower in 17-hpf *polr1a* mutant embryos than in wild-type controls. This reduction persisted in 24-hpf *polr1a* mutant embryos. Consistent with this reduction, immunostaining for HuC revealed that the cranial ganglia,

**Table 1. Key Features of Individuals with *POLR1A* Mutations**

| | Affected Individual | | |
|---|---|---|---|
| | **1A1** | **1A2** | **1A3** |
| *POLR1A* mutation[a] | c.1777G>C | c.3649delC | c.3895G>T |
| POLR1A variant | p.Glu593Gln | p.Gln1217Argfs*10 | p.Val1299Phe |
| Craniofacial features | ablepharon, absent zygoma, bilateral anotia, cleft palate, underdeveloped maxilla, micrognathia (severe) | bilateral choanal atresia, upper and lower eyelid clefts, microcephaly | down-slanting palpebral fissures, malar flattening, unilateral microtia, micrognathia (mild) |
| Limb features | bowed femora, flared metaphyses (lower extremities), dysplastic acetabulae, delayed ossification of epiphyses | none | short, broad fingers and toes |
| Developmental features | essentially normal at 2 years of age (mild communication delay) | normal at 6 years of age | normal at 52 years of age |
| Other | short stature | patent ductus arteriosus | – |

[a]GenBank: NM_015425.3.

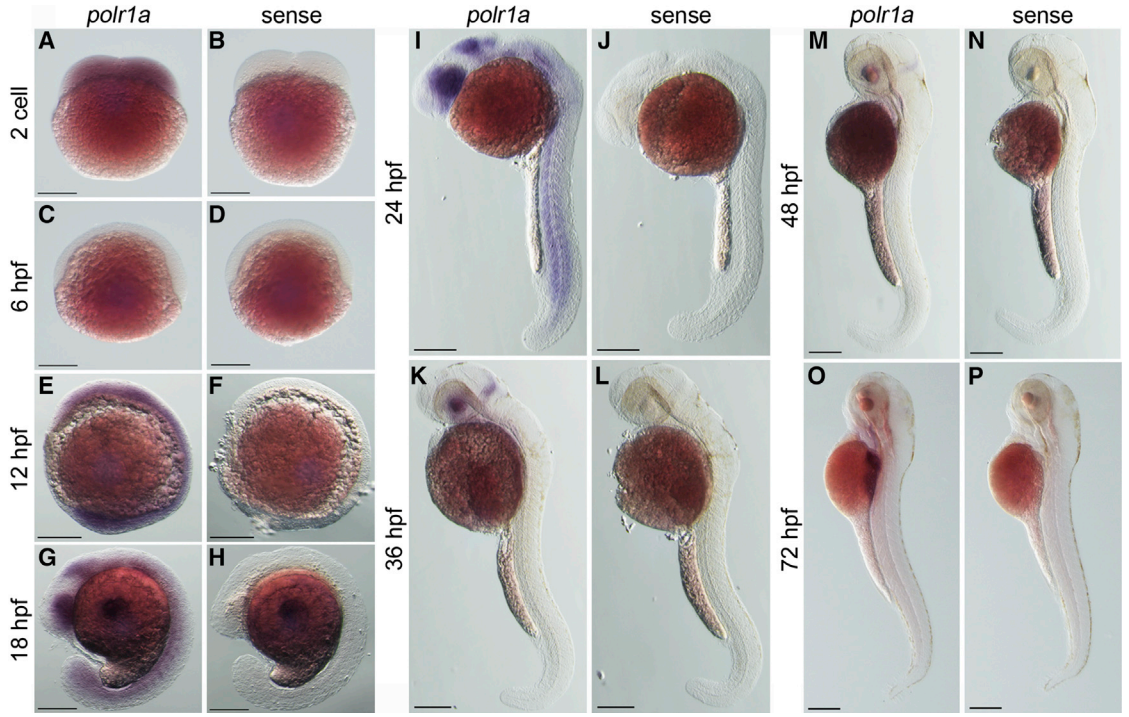


**Figure 3. In Situ Hybridization for *polr1a* at Various Zebrafish Stages Reveals a Dynamic Expression Pattern**
Maternal expression of *polr1a* was present at the 2-cell stage (A) but was not detected at 6 hpf (C). *polr1a* was ubiquitously expressed at 12 hpf (E), coincident with early NCC migration, and was expressed at 18 hpf in regions of the brain, eye, and somites (G). At 24 hpf, expression was present in the eye, midbrain-hindbrain boundary, otic vesicle, and somites (I). Beyond 36 hpf, expression was much reduced and was present in the lens of the eye and the midbrain-hindbrain boundary (K). The same expression was seen at 48 hpf (M), at which time additional expression was observed in the developing liver, which was clearly present at 72 hpf (O). The sense probe (B, D, F, H, J, L, N, and P) showed no signal at each stage examined. Scale bars represent 200 μm.

derived in part from *sox10*-positive NCCs, were hypoplastic in 3-dpf *polr1a* mutant embryos (Figure 5).

Similar to the reduction in *sox10*-labeled neurogenic precursor cells, a striking reduction in NCC-derived cartilage precursors was denoted via *sox9a* expression in 24-hpf *polr1a* mutant embryos (Figure 6). Furthermore, the expression of *dlx2a*, a marker of NCCs within the branchial arches, illustrated smaller and fewer branchial arches in *polr1a* mutants than in wild-type fish (four in mutants versus five in wild-type fish; Figure 6). Collectively, the reduction in *sox9-*, *sox10-*, and *dlx2*-labeled NCCs and the hypoplasia of the cranial ganglia, branchial arches, and jaw strongly support that NCC deficiency underlies the cranioskeletal defects observed in *polr1a* mutant embryos and in humans with acrofacial dysostosis, Cincinnati type.

The NCC deficiency could arise through perturbation of NCC progenitor development at the induction or migration stages. To discriminate between these possibilities, we assayed for apoptosis via TUNEL staining and for migrating NCCs in *polr1a; sox10:gfp* transgenic embryos at 14 hpf and also via Sox10 immunostaining in 24-hpf embryos. Early in NCC migration, at 14 hpf, *polr1a*$^{hi3639Tg/hi3639Tg}$*; sox10:gfp* embryos displayed more apoptosis than did wild-type controls (Figures 7A–7D). However, the TUNEL stain did not significantly co-localize with *sox10:gfp* expression, suggesting that the migratory NCC population was not undergoing apoptosis. Confirming these observations, at 24 hpf, apoptosis was present within the neural tube (Figures 7E–7J). Cross-sections through the neural tube revealed elevated apoptosis in the dorsal NCC progenitor domain (Figures 7H and 7J). These observations suggest that *polr1a* is required for neuroepithelial cell survival and the generation of NCCs but is not essential for the viability of migrating NCCs. Thus, the NCC deficiency in *polr1a* mutant embryos is mainly due to a reduction in the NCC progenitor pool, which diminishes the generation of migratory NCCs.

Polr1a composes the largest subunit of RNA polymerase I, which plays a key role in transcribing ribosomal RNA during the process of ribosome biogenesis. Given that ribosome biogenesis is essential for cell growth and proliferation[26] and that rDNA transcription is one of the rate-limiting steps of ribosome biogenesis,[27,28] we hypothesized that *polr1a* might regulate NCC progenitor cell survival in zebrafish by playing a key role in rDNA transcription. We determined the levels of rRNA transcription via qRT-PCR in 24-hpf embryos with primers designed against regions of the initial, unprocessed transcript (47S). All three regions of the unprocessed transcript were significantly reduced ($p < 0.01$) in *polr1a*$^{hi3639Tg/hi3639Tg}$ embryos, such that their production levels were less than half of those in wild-type controls (Figure 8). Furthermore, the 18S transcript, which includes both the stable

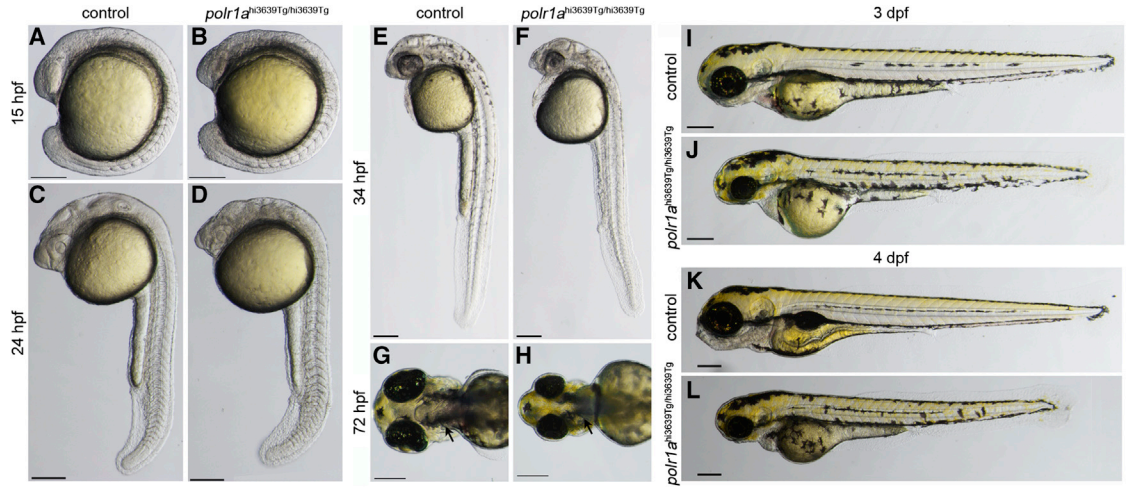


**Figure 4. Phenotype of *polr1a*$^{hi3639Tg/hi3639Tg}$ Zebrafish from 15 hpf to 4 dpf**
At 15 hpf, compared to wild-type siblings (A), mutant embryos first appeared with a grainy and irregular shape to the anterior region (B). This persisted through 24 hpf, when the cranial phenotype was more pronounced, the eyes were smaller, and the somites were wider (D) than those in wild-type siblings (C). At 34 hpf, pigment formation was clearly slower in mutant embryos than in wild-type siblings (E), and a bit of pericardial edema began to appear in mutant embryos (F). By 72 hpf, there was a clear lack of the ceratohyal and ceratobranchial cartilage (arrows point to cartilage in G and to the absence of these elements in H). Mutant embryos were smaller than wild-type siblings at 3 dpf (I and J) and 4 dpf (K and L). They showed much smaller eyes and otic vesicles and very small pectoral fins, failed to inflate their swim bladder, and had varying degrees of pericardial edema. Some mutants died by 4 dpf, and others died at 5 dpf, which was most likely due to cardiovascular defects. Scale bars represent 200 μm.

processed form and the unprocessed 47S, was also considerably reduced in *polr1a*$^{hi3639Tg/hi3639Tg}$ embryos. These results indicate that 47S production is disrupted in *polr1a* mutant embryos, compromising ribosome biogenesis and consequently NCC progenitor survival.

Deficient ribosome biogenesis is known to cause nucleolar stress activation of p53.[29] Therefore, we hypothesized that the cell death observed in *polr1a* mutant embryos might be p53 dependent. We examined *polr1a* mutant embryos for activation of *tp53* and Tp53 via qRT-PCR and immunoblot, respectively. *tp53* transcript levels were 4-fold higher in 24-hpf *polr1a* mutant embryos than in wild-type controls, and the protein levels showed a 1.2-fold increase at 4 dpf (Figures 8B and 8C).

## Discussion

*POLR1A* encodes subunit A190, the largest subunit of RNA polymerase I, which plays a key role in transcribing ribosomal RNA during the process of ribosome biogenesis. *S. cerevisiae* and human A190 proteins are 40%

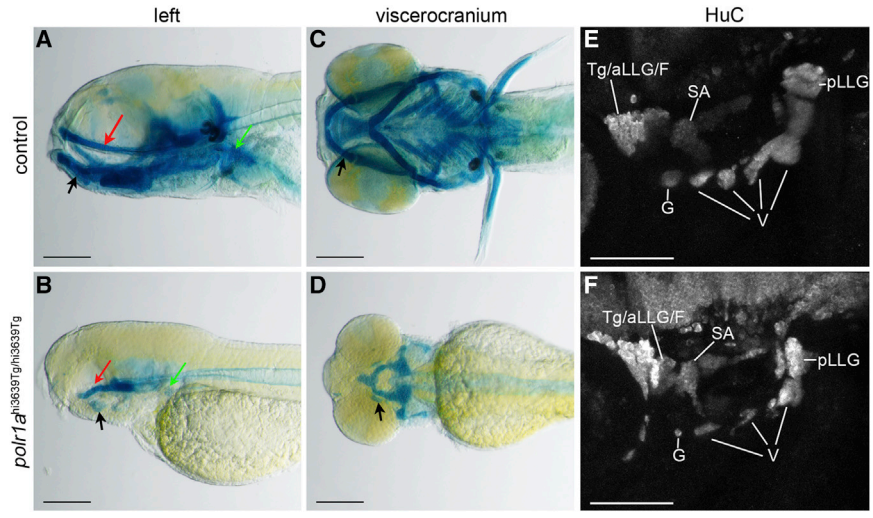


**Figure 5. *polr1a*$^{hi3639Tg/hi3639Tg}$ Embryos Show Reduced Formation of NCC-Derived Elements**
Alcian blue staining at 5 dpf (A–D) shows that whereas elements of the neurocranium (such as the trabeculae) were present in both wild-type and mutant embryos (red arrows), very little of the viscerocranium was present in mutant embryos (D). Some cartilage in the region of the jaw was faintly present in mutant embryos. It is possible that this could be Meckel's cartilage (black arrows). A smaller region of Alcian blue staining posterior to the black arrow could potentially be the ceratohyal. There was also a small remnant of staining in the pectoral fin (green arrows in A and B) in the mutant embryos. Scale bars in (A)–(D) represent 200 μm. Immunostaining for HuC at 82 hpf (E and F) shows reduced and delayed neuronal development in mutant embryos. All cranial ganglia were present in mutant embryos (F), but they were smaller than those in control siblings (E). Abbreviations are as follows: Tg, trigeminal ganglion; aLLG, anterior lateral line ganglion; F, facial ganglion complex; SA, statoacoustic ganglion; pLLg, posterior lateral line ganglion; G, glossopharyngeal ganglion; V, vagal ganglia. Scale bars in (E) and (F) represent 100 μm.

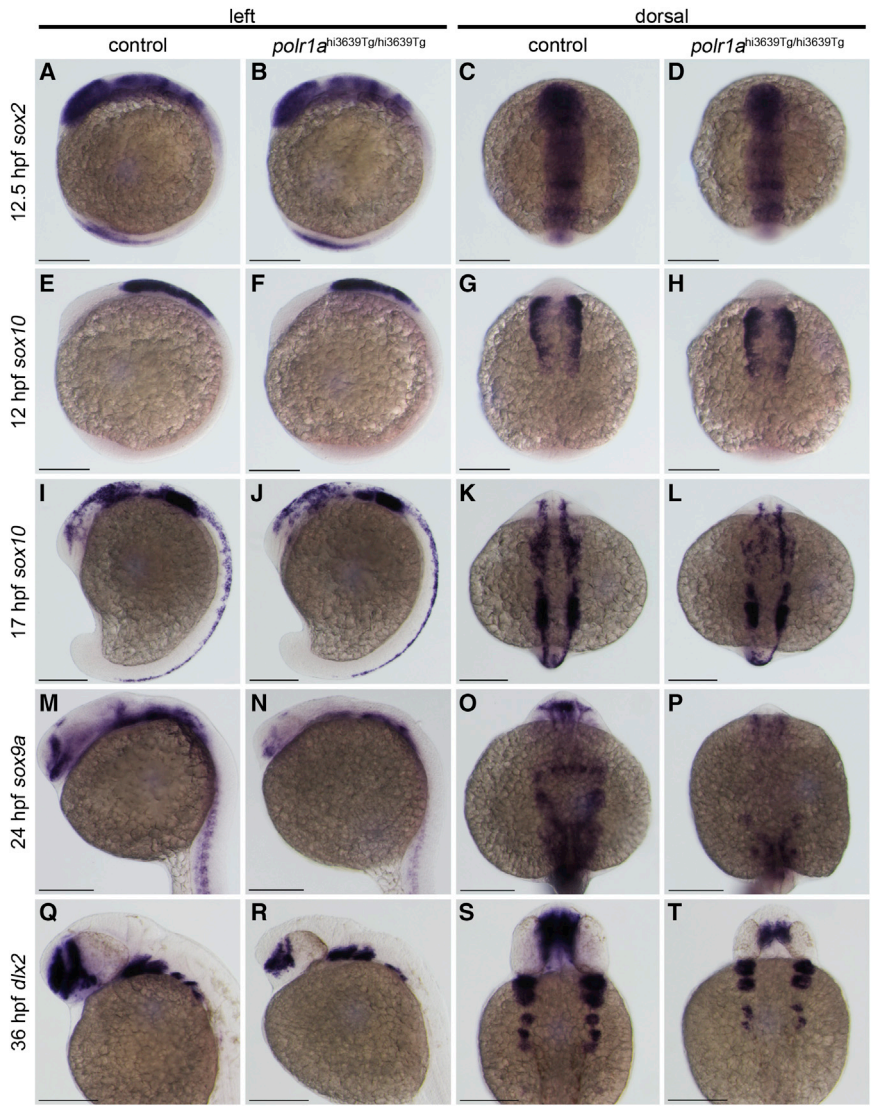


**Figure 6. In Situ Hybridization for Markers of NCC Development**

In situ hybridization for *sox2* (A–D) and *sox10* (E–H) at 12 hpf shows that levels of NCC induction were relatively similar between mutant embryos and wild-type siblings. At 17 hpf, soon after the onset of a visible mutant phenotype, the level of *sox10* staining was lower in mutant embryos (J and L) than in wild-type controls (I and K), indicating a reduced migratory NCC population. By 24 hpf, the population of cartilage precursors labeled by *sox9a* (M–P) showed a strong reduction throughout mutant embryos, especially in the pharyngeal arches (N and P). The population of NCCs in the pharyngeal arches (shown by *dlx2a* in situ at 36 hpf in Q–T) was also reduced in mutant embryos (R and T). The mutant embryos showed overall diminished staining and a lack of the fifth arch. Scale bars represent 200 μm.

homologous overall and have increased homology in the active site and DNA-binding cleft domains (Table S7). The crystal structure of RNA polymerase I in *S. cerevisiae* revealed that subunits A190 and A135 interface to form a composite active site. Subunit A190 forms a "shelf" module that interacts with the "core" module, subunit A135. The cleft between A190 and A135 must contract, via rotation of the core and shelf modules, so that a conserved aspartate loop within the cleft can bind two catalytic metal ions and the RNA 3′ end.[30] Here, we have presented three individuals with phenotypes ranging from mild isolated mandibulofacial dysostosis to severe acrofacial dysostosis and heterozygous variants in *POLR1A*. Supporting the hypothesis that POLR1A dysfunction causes these phenotypes, in vivo studies of *polr1a* expression and function in zebrafish demonstrated that zebrafish *polr1a* mutants exhibit cranioskeletal defects that mimic the severe phenotype found in individual 1A1. Notably, the tissues that were affected in both affected humans and mutant zebrafish correlate with the domains of enriched *polr1a* expression during embryogenesis. Taken together, our data indicate that *polr1a* loss of function compromises rDNA transcription, one of the rate-limiting steps in the process of ribosome biogenesis. Deficient ribosome biogenesis in turn leads to activation of p53-dependent cell death, which diminishes the generation of migrating NCCs and results in the cranioskeletal hypoplasia characteristic of acrofacial dysostosis, Cincinnati type (Figure S3). Our data are consistent with those of in vitro studies that demonstrated that in human cancer cells, *POLR1A* silencing leads to increased apoptosis via p53-dependent pathways.[31,32] Collectively, these studies demonstrate the critical importance of *polr1a* in cell survival, as well as in bone and cartilage development during embryogenesis. Furthermore, they support the classification of acrofacial dysostosis, Cincinnati type as a ribosomopathy.

The specific mechanism underpinning femoral bowing, metaphyseal flaring, and delayed epiphyseal ossification in individual 1A1 is not yet understood. However, limb abnormalities are a characteristic feature of Nager syndrome, and femoral bowing has been observed in association with bent-bone dysplasia syndrome (BBDS [MIM: 614592]). Although Nager syndrome is caused by mutations in *SF3B4* (MIM: 605593)[8] and BBDS is caused by mutations in *FGFR2* (MIM: 176943),[33] both conditions are associated with perturbed ribosome biogenesis. Interestingly, RUNX2 is essential for osteoblast differentiation and has been shown to associate with the RNA polymerase I regulator complex and repress the rDNA promoter and thus influence rRNA synthesis.[34] Furthermore, mutations in

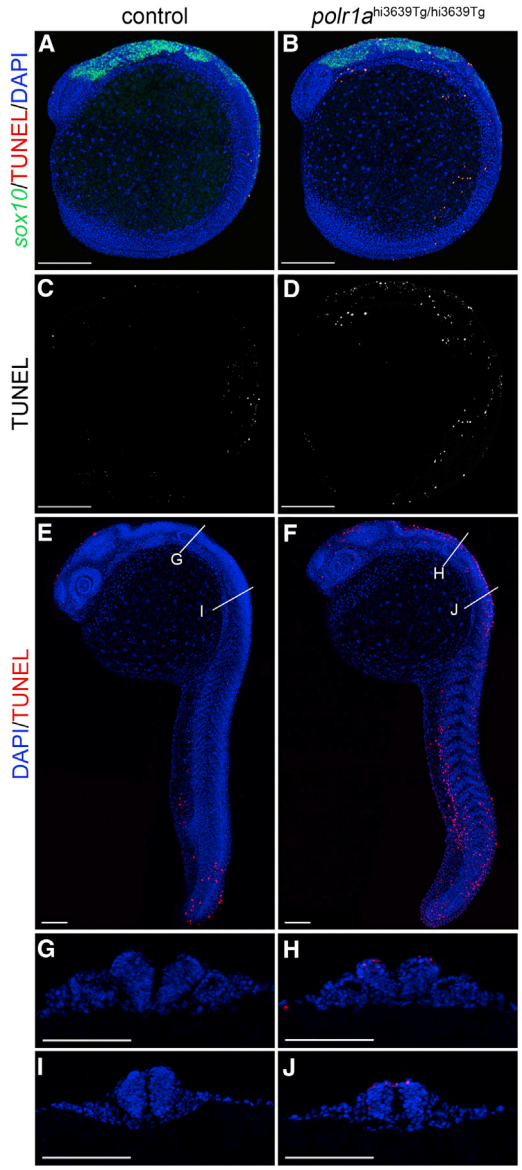


**Figure 7. TUNEL Staining Reveals Increased Cell Death in Mutant Embryos**

Cell death was present throughout the *polr1a*$^{hi3639Tg/hi3639Tg}$ embryos at both 14 and 24 hpf and was especially high within the neural tube. At 14 hpf (A–D), TUNEL staining did not significantly co-localize with the migratory NCC population, as shown by *sox10:gfp* expression. Scale bars in (A)–(D) represent 200 μm. At 24 hpf (E–J), cross-sections through the embryos showed cell death in the dorsal portion of the neural tube in mutant embryos (H and J), whereas control embryos did not show cell death in this location (G and I). Scale bars in (E)–(J) represent 100 μm.

*RUNX2* (MIM: 600211) are known to cause cleidocranial dysplasia (MIM: 119600), which is characterized by craniskeletal anomalies together with decreased bone density.[35] Together, these studies demonstrate an important role for ribosome biogenesis in limb and general skeletal development[7] and imply that the limb skeletal defects associated with acrofacial dysostosis, Cincinnati type might also be caused by perturbed ribosome biogenesis.

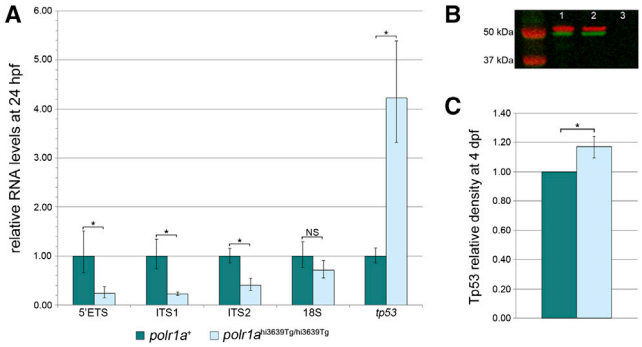


**Figure 8. qRT-PCR for rRNA Transcripts Shows a Significant Reduction in *polr1a*$^{hi3639Tg/hi3639Tg}$ Embryos, whereas *tp53* Levels Are Increased**

(A) The level of ITS1 in mutant embryos was 23% of that in wild-type siblings, the level of ITS2 was 41%, and the level of the 5′ externally transcribed sequence (ETS) was 24%. The 18S levels also tended to be lower in mutants (71%) than in wild-types (100%), but this difference was not significant ($p = 0.095$). qRT-PCR showed a 4-fold increase in the transcription of *tp53* in *polr1a* mutant embryos at 24 hpf, which is when rRNA transcription diminished. Error bars represent 95% confidence intervals.

(B) Immunoblot analysis was used to determine levels of Tp53. Lane 1 shows the control, lane 2 shows the *polr1a*$^{hi3639Tg/hi3639Tg}$ embryo, and lane 3 shows the negative control. The red signal is α-tubulin, and the green signal is Tp53.

(C) Quantification of immunoblots in ImageJ revealed that the levels of Tp53 were significantly higher ($p = 0.007$) in mutant embryos than in wild-type siblings at 4 dpf. *$p < 0.01$. Error bars represent 95% confidence intervals.

The phenotypic specificity observed in humans and zebrafish with abnormal function of *POLR1A* and *polr1a*, respectively, suggests that certain tissues require threshold levels of ribosomes for normal development or that they might be particularly sensitive to perturbations in ribosome biogenesis. This phenomenon appears to be common to ribosomopathies. Nager syndrome, Treacher Collins syndrome, and Diamond Blackfan anemia all involve similar craniofacial malformations consistent with mandibulofacial dysostosis, but they are also associated with syndrome-specific defects such as limb or blood anomalies despite disruptions of the same global process.[6,7,36] Differential regulation of rRNA, ribosomal protein activity, or protein translation in distinct tissues could mechanistically underlie the phenotypic specificity of each ribosomopathy despite disruption of the same putatively ubiquitous ribosome-biogenesis process. This variability in threshold ribosome levels might also underlie the phenotypic variability between affected individuals if certain mutations cause less of a disturbance to ribosome biogenesis.

Further study of mutation-specific *POLR1A* dysfunction might help elucidate the specific roles of ribosome biogenesis in chondrogenesis and osteogenesis and account for the disparate phenotypes of the three individuals we have described here. The variable severity might also correlate with the location or type of mutation in *POLR1A* or alternatively be due to as yet unidentified genetic modifiers, as has been suggested to underlie phenotypic

variability in Treacher Collins syndrome.[37] It is of particular interest that the most severely affected individual, IA-1, has a missense variant in the catalytic site (p.Glu593Gln) of the protein A190 (Figure S4). The wild-type glutamic acid residue at position 593 is adjacent to a highly conserved D-D-D motif, which forms an aspartate loop and coordinates binding of two catalytic metal ions when the protein is in its contracted, active state.[30] Individual 1A2, with an intermediate phenotype between those of 1A1 and 1A3, has a frameshift variant predicted to truncate the protein and thus remove a portion of the second cleft domain and all of the jaw, expander, and third cleft domains (Figure S4). Individual 1A3, with the mildest craniofacial phenotype, has a missense variant affecting the jaw domain of the protein (Figure S4). The expander, which is connected to the jaw, stabilizes the cleft between A190 and A135 when it is open and inactive.[10] Although the frameshift variant in individual 1A2 was inherited from her very mildly affected father, this does not preclude the variant from causality. It is well known that the phenotype of Treacher Collins syndrome is variable, given that documented cases of family members have identical mutations with markedly different expression.[38] Individuals 1A2 and 1A3 did not undergo exome sequencing for excluding the possibility of additional genetic diagnoses. However, the index affected individual, 1A1, did undergo exome analysis, and no additional putative variants were identified. Therefore, the likelihood of an alternative primary genetic explanation for the phenotypes of 1A2 and 1A3 is extremely low.

In conclusion, our description of the etiology and pathogenesis of acrofacial dysostosis, Cincinnati type as a ribosomopathy arising from mutations in *POLR1A* provides an opportunity to gain further insight into the impact of disordered ribosome biogenesis on craniofacial and limb skeletal development. Additionally, it represents a starting point for exploring possible avenues for prevention, similar to what has been accomplished with Treacher Collins syndrome.[4,5]

## Supplemental Data

Supplemental Data include four figures and seven tables and can be found with this article online at http://dx.doi.org/10.1016/j.ajhg.2015.03.011.

## Acknowledgments

We are grateful to the affected individuals and their families for participating in this study. We thank Daniela Falkenstein for excellent technical assistance, Angela Newton for assistance in cloning zebrafish *polr1a*, and Diana Baumann and the Reptile and Aquatic Facility at the Stowers Institute for excellent zebrafish breeding, maintenance, and care. We would like to thank the Nancy Hopkins laboratory for generating the *polr1a*$^{hi3639Tg}$ zebrafish and Dr. Adam Amsterdam for providing primer sequences for genotyping. The *sox10:gfp* zebrafish were a kind gift from Dr. Thomas Schilling. This work was supported by German Federal Ministry of Education and Research (BMBF) grants 01GM1211B and 01GM1109B to D.W., a National Research Service Award F31 (DE023017) fellowship from the National Institute for Dental and Craniofacial Research to K.E.N.W., Stowers Institute for Medical Research funding to P.A.T., and National Institute for Dental and Craniofacial Research grant DE016082 to P.A.T.

Received: January 21, 2015
Accepted: March 19, 2015
Published: April 23, 2015

## Web Resources

The URLs for data presented herein are as follows:

Clustal Omega, http://www.ebi.ac.uk/Tools/msa/clustalo/
GenBank, http://www.ncbi.nlm.nih.gov/genbank/
OMIM, http://www.omim.org/

## References

1. Stoll, C., Dott, B., Roth, M.P., and Alembik, Y. (1989). Birth prevalence rates of skeletal dysplasias. Clin. Genet. *35*, 88–92.
2. Wieczorek, D. (2013). Human facial dysostoses. Clin. Genet. *83*, 499–510.
3. Valdez, B.C., Henning, D., So, R.B., Dixon, J., and Dixon, M.J. (2004). The Treacher Collins syndrome (TCOF1) gene product is involved in ribosomal DNA gene transcription by interacting with upstream binding factor. Proc. Natl. Acad. Sci. USA *101*, 10709–10714.
4. Jones, N.C., Lynn, M.L., Gaudenz, K., Sakai, D., Aoto, K., Rey, J.P., Glynn, E.F., Ellington, L., Du, C., Dixon, J., et al. (2008). Prevention of the neurocristopathy Treacher Collins syndrome through inhibition of p53 function. Nat. Med. *14*, 125–133.
5. Dixon, J., Jones, N.C., Sandell, L.L., Jayasinghe, S.M., Crane, J., Rey, J.P., Dixon, M.J., and Trainor, P.A. (2006). Tcof1/Treacle is required for neural crest cell formation and proliferation deficiencies that cause craniofacial abnormalities. Proc. Natl. Acad. Sci. USA *103*, 13403–13408.
6. Trainor, P.A., and Andrews, B.T. (2013). Facial dysostoses: Etiology, pathogenesis and management. Am. J. Med. Genet. C. Semin. Med. Genet. *163C*, 283–294.
7. Trainor, P.A., and Merrill, A.E. (2014). Ribosome biogenesis in skeletal development and the pathogenesis of skeletal disorders. Biochim. Biophys. Acta *1842*, 769–778.
8. Bernier, F.P., Caluseriu, O., Ng, S., Schwartzentruber, J., Buckingham, K.J., Innes, A.M., Jabs, E.W., Innis, J.W., Schuette, J.L., Gorski, J.L., et al.; FORGE Canada Consortium (2012). Haploinsufficiency of SF3B4, a component of the pre-mRNA spliceosomal complex, causes Nager syndrome. Am. J. Hum. Genet. *90*, 925–933.
9. DePristo, M.A., Banks, E., Poplin, R., Garimella, K.V., Maguire, J.R., Hartl, C., Philippakis, A.A., del Angel, G., Rivas, M.A., Hanna, M., et al. (2011). A framework for variation discovery and genotyping using next-generation DNA sequencing data. Nat. Genet. *43*, 491–498.
10. Li, H., and Durbin, R. (2009). Fast and accurate short read alignment with Burrows-Wheeler transform. Bioinformatics *25*, 1754–1760.
11. Sievers, F., Wilm, A., Dineen, D., Gibson, T.J., Karplus, K., Li, W., Lopez, R., McWilliam, H., Remmert, M., Söding, J., et al.

(2011). Fast, scalable generation of high-quality protein multiple sequence alignments using Clustal Omega. Mol. Syst. Biol. *7*, 539.
12. McWilliam, H., Li, W., Uludag, M., Squizzato, S., Park, Y.M., Buso, N., Cowley, A.P., and Lopez, R. (2013). Analysis Tool Web Services from the EMBL-EBI. Nucleic Acids Res. *41*, W597–W600.
13. Goujon, M., McWilliam, H., Li, W., Valentin, F., Squizzato, S., Paern, J., and Lopez, R. (2010). A new bioinformatics analysis tools framework at EMBL-EBI. Nucleic Acids Res. *38*, W695–W699.
14. Kimmel, C.B., Ballard, W.W., Kimmel, S.R., Ullmann, B., and Schilling, T.F. (1995). Stages of embryonic development of the zebrafish. Dev. Dyn. *203*, 253–310.
15. Amsterdam, A., Burgess, S., Golling, G., Chen, W., Sun, Z., Townsend, K., Farrington, S., Haldi, M., and Hopkins, N. (1999). A large-scale insertional mutagenesis screen in zebrafish. Genes Dev. *13*, 2713–2724.
16. Amsterdam, A., Nissen, R.M., Sun, Z., Swindell, E.C., Farrington, S., and Hopkins, N. (2004). Identification of 315 genes essential for early zebrafish development. Proc. Natl. Acad. Sci. USA *101*, 12792–12797.
17. Hoffman, T.L., Javier, A.L., Campeau, S.A., Knight, R.D., and Schilling, T.F. (2007). Tfap2 transcription factors in zebrafish neural crest development and ectodermal evolution. J. Exp. Zoolog. B Mol. Dev. Evol. *308*, 679–691.
18. Walker, M.B., and Kimmel, C.B. (2007). A two-color acid-free cartilage and bone stain for zebrafish larvae. Biotech. Histochem. *82*, 23–28.
19. Westerfield, M. (2000). The Zebrafish Book. A Guide for the Laboratory Use of Zebrafish (*Danio rerio*), Fourth Edition (University of Oregon Press). http://zfin.org/zf_info/zfbook/zfbk.html.
20. Crump, J.G., Swartz, M.E., and Kimmel, C.B. (2004). An integrin-dependent role of pouch endoderm in hyoid cartilage development. PLoS Biol. *2*, E244.
21. Azuma, M., Toyama, R., Laver, E., and Dawid, I.B. (2006). Perturbation of rRNA synthesis in the bap28 mutation leads to apoptosis mediated by p53 in the zebrafish central nervous system. J. Biol. Chem. *281*, 13309–13316.
22. Wieczorek, D., Newman, W.G., Wieland, T., Berulava, T., Kaffe, M., Falkenstein, D., Beetz, C., Graf, E., Schwarzmayr, T., Douzgou, S., et al. (2014). Compound heterozygosity of low-frequency promoter deletions and rare loss-of-function mutations in TXNL4A causes Burn-McKeown syndrome. Am. J. Hum. Genet. *95*, 698–707.
23. Abecasis, G.R., Auton, A., Brooks, L.D., DePristo, M.A., Durbin, R.M., Handsaker, R.E., Kang, H.M., Marth, G.T., and McVean, G.A.; 1000 Genomes Project Consortium (2012). An integrated map of genetic variation from 1,092 human genomes. Nature *491*, 56–65.
24. Tennessen, J.A., Bigham, A.W., O'Connor, T.D., Fu, W., Kenny, E.E., Gravel, S., McGee, S., Do, R., Liu, X., Jun, G., et al.; Broad GO; Seattle GO; NHLBI Exome Sequencing Project (2012). Evolution and functional impact of rare coding variation from deep sequencing of human exomes. Science *337*, 64–69.
25. Noden, D.M., and Trainor, P.A. (2005). Relations and interactions between cranial mesoderm and neural crest populations. J. Anat. *207*, 575–601.
26. Thomas, G. (2000). An encore for ribosome biogenesis in the control of cell proliferation. Nat. Cell Biol. *2*, E71–E72.
27. Laferté, A., Favry, E., Sentenac, A., Riva, M., Carles, C., and Chédin, S. (2006). The transcriptional activity of RNA polymerase I is a key determinant for the level of all ribosome components. Genes Dev. *20*, 2030–2040.
28. Hannan, K.M., Brandenburger, Y., Jenkins, A., Sharkey, K., Cavanaugh, A., Rothblum, L., Moss, T., Poortinga, G., McArthur, G.A., Pearson, R.B., and Hannan, R.D. (2003). mTOR-dependent regulation of ribosomal gene transcription requires S6K1 and is mediated by phosphorylation of the carboxy-terminal activation domain of the nucleolar transcription factor UBF. Mol. Cell. Biol. *23*, 8862–8877.
29. Rubbi, C.P., and Milner, J. (2003). Disruption of the nucleolus mediates stabilization of p53 in response to DNA damage and other stresses. EMBO J. *22*, 6068–6077.
30. Engel, C., Sainsbury, S., Cheung, A.C., Kostrewa, D., and Cramer, P. (2013). RNA polymerase I structure and transcription regulation. Nature *502*, 650–655.
31. Donati, G., Bertoni, S., Brighenti, E., Vici, M., Treré, D., Volarevic, S., Montanaro, L., and Derenzini, M. (2011). The balance between rRNA and ribosomal protein synthesis up- and downregulates the tumour suppressor p53 in mammalian cells. Oncogene *30*, 3274–3288.
32. Donati, G., Brighenti, E., Vici, M., Mazzini, G., Treré, D., Montanaro, L., and Derenzini, M. (2011). Selective inhibition of rRNA transcription downregulates E2F-1: a new p53-independent mechanism linking cell growth to cell proliferation. J. Cell Sci. *124*, 3017–3028.
33. Neben, C.L., Idoni, B., Salva, J.E., Tuzon, C.T., Rice, J.C., Krakow, D., and Merrill, A.E. (2014). Bent bone dysplasia syndrome reveals nucleolar activity for FGFR2 in ribosomal DNA transcription. Hum. Mol. Genet. *23*, 5659–5671.
34. Young, D.W., Hassan, M.Q., Pratap, J., Galindo, M., Zaidi, S.K., Lee, S.H., Yang, X., Xie, R., Javed, A., Underwood, J.M., et al. (2007). Mitotic occupancy and lineage-specific transcriptional control of rRNA genes by Runx2. Nature *445*, 442–446.
35. Otto, F., Kanegane, H., and Mundlos, S. (2002). Mutations in the RUNX2 gene in patients with cleidocranial dysplasia. Hum. Mutat. *19*, 209–216.
36. Hannan, K.M., Sanij, E., Rothblum, L.I., Hannan, R.D., and Pearson, R.B. (2013). Dysregulation of RNA polymerase I transcription during disease. Biochim. Biophys. Acta *1829*, 342–360.
37. Dixon, J., and Dixon, M.J. (2004). Genetic background has a major effect on the penetrance and severity of craniofacial defects in mice heterozygous for the gene encoding the nucleolar protein Treacle. Dev. Dyn. *229*, 907–914.
38. Hansen, M., Lucarelli, M.J., Whiteman, D.A., and Mulliken, J.B. (1996). Treacher Collins syndrome: phenotypic variability in a family including an infant with arhinia and uveal colobomas. Am. J. Med. Genet. *61*, 71–74.